Structure and conformational change of a replication protein A heterotrimer bound to ssDNA

Jie Fan[1] and Nikola P. Pavletich[2,3]

[1]Sloan-Kettering Division, Joan and Sanford I. Weill Graduate School of Medical Sciences, Cornell University, New York, New York 10065, USA; [2]Howard Hughes Medical Institute, Structural Biology Program, Memorial Sloan-Kettering Cancer Center, New York, New York 10065, USA

Replication protein A (RPA) is the main eukaryotic ssDNA-binding protein with essential roles in DNA replication, recombination, and repair. RPA maintains the DNA as single-stranded and also interacts with other DNA-processing proteins, coordinating their assembly and disassembly on DNA. RPA binds to ssDNA in two conformational states with opposing affinities for DNA and proteins. The RPA–protein interactions are compatible with a low DNA affinity state that involves DNA-binding domain A (DBD-A) and DBD-B but not with the high DNA affinity state that additionally engages DBD-C and DBD-D. The structure of the high-affinity RPA–ssDNA complex reported here shows a compact quaternary structure held together by a four-way interface between DBD-B, DBD-C, the intervening linker (BC linker), and ssDNA. The BC linker binds into the DNA-binding groove of DBD-B, mimicking DNA. The associated conformational change and partial occlusion of the DBD-A–DBA-B protein–protein interaction site establish a mechanism for the allosteric coupling of RPA–DNA and RPA–protein interactions.

[*Keywords*: DNA repair; DNA replication; RPA; ssDNA binding]

Supplemental material is available for this article.

Received May 21, 2012; revised version accepted August 29, 2012.

Replication protein A (RPA) is the primary ssDNA-binding factor in eukaryotes and is essential for most aspects of DNA metabolism, such as replication, repair, and recombination (Wold 1997; Iftode et al. 1999; Zou et al. 2006). RPA removes the ssDNA secondary structure that may otherwise interfere with DNA processing, maintains it as single-stranded, and protects it from nucleases. In addition, RPA plays a role in regulating and coordinating the assembly and disassembly of DNA-processing factors on ssDNA (Yuzhakov et al. 1999; Fanning et al. 2006). In replication, RPA coordinates the lagging strand polymerase switching from the low-fidelity polymerase α (Pol α), which extends the RNA primer of Okazaki fragments, to the high-fidelity Pol δ. This process, termed "handoff," is mediated by RPA sequentially binding to and releasing Pol α–primase, the replication factor C (RFC), and then Pol δ (Yuzhakov et al. 1999). During Okazaki fragment maturation, RPA coordinates the sequential action of the DNA2 and FEN1 flap endonucleases that remove the RNA primer (Bae et al. 2001; Stewart et al. 2008). RPA has analogous roles in DNA repair pathways as well. In nucleotide excision repair (NER), RPA recruits the XPG and ERCC1-XPF endonucleases to the lesion and coordinates the selection of sites for the dual incision reactions (Fanning et al. 2006; Zou et al. 2006). During the repair of DNA double-strand breaks (DSBs) by homologous recombination (HR), RPA sequesters the ssDNA of the resected DSB, allowing the formation of the RAD51–ssDNA nucleoprotein filament to be regulated by the HR mediator factors Rad52 and BRCA2 (New et al. 1998; Yang et al. 2005).

RPA is a heterotrimeric complex of RPA70, RPA32, and RPA14. These subunits consist primarily of the OB (oligonucleotide/oligosaccharide-binding) fold, an ~120-residue β barrel of five strands (Murzin 1993; Flynn and Zou 2010). RPA70 consists of four OB folds, whereas RPA32 has one OB fold followed by an ~60-amino-acid winged helix (WH) domain. RPA14 has a single OB fold. Heterotrimerization is mediated primarily through a three-helix bundle formed by a C-terminal α helix from each subunit (Iftode et al. 1999; Bochkareva et al. 2002).

RPA binds to ssDNA in two modes that differ in the length and affinity of the bound DNA and also in the quaternary conformation of RPA and in its protein–protein interaction activities (Fanning et al. 2006). A low-affinity mode has an occluded binding site of ~8 nucleotides (nt)

[3]**Corresponding author**
E-mail pavletin@mskcc.org
Article is online at http://www.genesdev.org/cgi/doi/10.1101/gad.194787.112.

and a dissociation constant (Kd) of ~50 nM (Kim et al. 1994; Iftode et al. 1999; Bochkareva et al. 2002). This mode, referred to as the 8-nt mode, involves only the second and third RPA70 OB folds (termed DBD-A [for DNA-binding domain A] and DBD-B) contacting the ssDNA (Bochkarev et al. 1997; Arunkumar et al. 2003). The high-affinity mode has an occluded binding site of ~30 nt and a Kd of ~0.05 nM (termed the 30-nt mode) (Blackwell and Borowiec 1994; Wyka et al. 2003). This mode engages, in addition to DBD-A and DBD-B, the third RPA70 OB fold (DBD-C) and the single RPA32 OB fold (DBD-D) in ssDNA contacts (Bochkareva et al. 1998, 2002; Brill and Bastin-Shanower 1998; Lao et al. 1999; Wyka et al. 2003). DBD-C contributes the majority of the increase in affinity and can bind to DNA weakly in the absence of DBD-A–DBA-B (Brill and Bastin-Shanower 1998; Lao et al. 1999). The two modes are thought to reflect a sequential process of RPA–ssDNA association and dissociation that facilitates the initial binding of RPA to ssDNA and the displacement of RPA by other factors during DNA processing (Fanning et al. 2006).

The conformational changes associated with the two binding modes involve the relative arrangement of the DBDs and the structures of the linker segments in between. In the absence of DNA, the interdomain linkers between DBD-A and DBD-B and also between DBD-B and DBD-C are highly susceptible to limited proteolysis (Gomes et al. 1996; Bochkareva et al. 2002). Nuclear magnetic resonance (NMR) and crystallographic analyses of apo DBD-A–DBD-B fragments are consistent with the linker between DBD-A and DBD-B being a flexible tether (Bochkareva et al. 2001; Arunkumar et al. 2003). On ssDNA binding, the DBD-A–DBD-B linker is protected from proteolysis in both the 8- and 30-nt modes (Gomes et al. 1996). In the crystal structure of DBD-A–DBD-B bound to a $(dC)_8$ oligonucleotide, this linker becomes well ordered, and the DBD-A and DBD-B domains interact with each other (Bochkarev et al. 1997). In contrast, the linker between DBD-B and DBD-C becomes protease-resistant only in the 30-nt mode, for which there is no structural information available (Gomes et al. 1996; Bochkareva et al. 2002).

The differences in the protein–protein interaction activities of the two modes map primarily to the DBD-A and DBD-B domains. A site (or sites) spanning these domains binds to a large number of DNA-processing factors, such as the replication protein Pol α–primase, the RAD52 HR protein, and the NER factor XPA (Braun et al. 1997; Jackson et al. 2002; Yang et al. 2002; Fanning et al. 2006). This site is also contacted by several viral replication initiator/helicase proteins, such as the simian virus 40 (SV40) T antigen (Tag) and the papillomavirus E1 (Han et al. 1999; Loo and Melendy 2004; Fanning et al. 2006). Studies with Tag, E1, and Pol α–primase have shown that these proteins can bind to apo-RPA or the 8-nt-mode RPA–ssDNA complex but not to the 30-nt RPA–ssDNA complex (Loo and Melendy 2004; Jiang et al. 2006). It has thus been suggested that RPA–protein interactions at this site are modulated allosterically by changes in the RPA conformation or quaternary structure that are induced by the transition from the 8- to the 30-nt-mode complex (Jiang et al. 2006). This allosteric link is thought to be important for the RPA-mediated handoff of ssDNA to successive factors, such as the polymerase switch on Okazaki fragments (Yuzhakov et al. 1999; Fanning et al. 2006). In addition, it is involved in the loading of RPA to ssDNA, at least in viral replication model systems (Loo and Melendy 2004; Jiang et al. 2006), and may play a role in its displacement during DNA processing (Fanning et al. 2006).

Here we report the 2.8-Å structure of the 30-nt-mode RPA–ssDNA complex and discuss the implications the structure has for understanding how the formation of the high-affinity RPA–ssDNA complex modulates RPA–protein interactions and how this coupling mediates the handoff process and the displacement of RPA by other DNA-processing factors.

Results

Overall structure of the 30-nt-mode RPA–ssDNA complex

For crystallization, the Rpa subunits from the fungus *Ustilago maydis* were truncated to remove the N-terminal OB fold of Rpa70 (OBN) and the C-terminal WH domain of Rpa32. These domains contain additional protein–protein interaction sites and do not appear to contribute to the DNA affinity of the 30-nt DNA-binding mode (Gomes and Wold 1996; Fanning et al. 2006). They are connected to the DNA-binding core through linkers that are longer and poorly conserved compared with the linkers between the DBD domains (Fig. 1A). The truncated Rpa binds to 32-nt-long ssDNA with the same affinity as intact Rpa (Supplemental Fig. S1). The truncated *U. maydis* Rpa was crystallized bound to oligodeoxythymide ssDNA of either 62 nt [$(dT)_{62}$] or 32 nt [$(dT)_{32}$], and the structures were refined at 2.8-Å and 3.1-Å resolution, respectively (Table 1). Both crystal forms contain two Rpa–ssDNA complexes in the asymmetric unit with very similar structures (Supplemental Fig. S2A).

The 30-nt-mode Rpa–ssDNA complex adopts a compact quaternary structure with the Rpa70 and Rpa32 subunits packing in a plane and the Rpa14 subunit extending beyond the surface of this plane. The DNA-binding grooves of the three Rpa70 OB folds (DBD-A, DBD-B, and DBD-C) and one Rpa32 OB fold (DBD-D) are positioned on the same face of the plane, opposite from where the Rpa14 subunit is (Fig. 1B,C).

Compared with the structures of the DBD-A–DBD-B-$(dC)_8$ complex and the apo-DBD-C–DBD-D–RPA14 heterotrimerization core, the 30-nt-mode structure contains a new interface that anchors these two portions of Rpa together. This interface involves DBD-B, DBD-C, ssDNA, and a 10-residue segment of the linker polypeptide between DBD-B and DBD-C (Fig. 1B,C). This linker segment (residues 441–450; hereafter, BC linker) is unstructured in the 8-nt binding mode and is absent from the structures of RPA fragments (Gomes and Wold 1996; Bochkarev et al. 1997, 2002). In the 30-nt-mode structure,

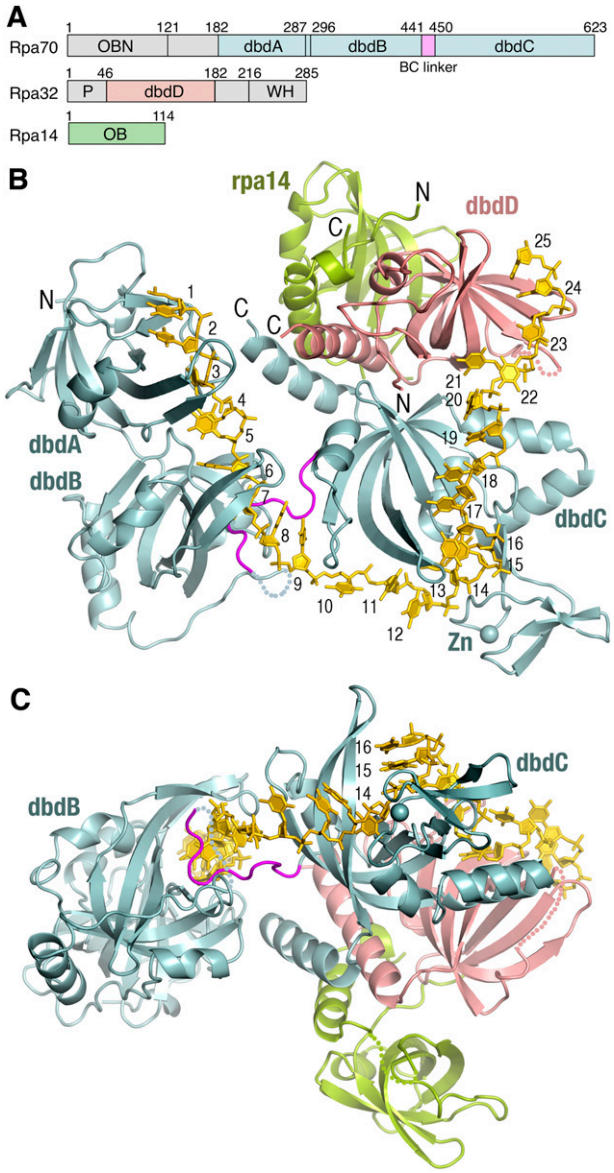

Figure 1. Structure of the Rpa heterotrimer bound to ssDNA. (*A*) Linear representation of *U. maydis* Rpa70, Rpa32, and Rpa14 proteins indicating the boundaries of their structural domains. The gray regions were excluded from the crystallized Rpa heterotrimer. (OBN) Rpa70 N-terminal OB fold; (WH) Rpa32 winged helix; (P) phosphorylation sites. (*B*) Overall structure of the complex, with Rpa70 colored light blue, Rpa32 in pink, Rpa14 colored green, ssDNA in yellow, and the BC linker colored magenta. The 25 ordered nucleotides of the oligo(dT)$_{32}$ ssDNA are numbered starting from the 5′ end. The N and C termini are labeled, and the Zn atom in DBD-C is shown as a sphere. (*C*) View rotated 180° about the horizontal axis of *B*, highlighting the planar arrangement of the DNA-binding grooves and the position of Rpa32 away from this plane.

it becomes well ordered (electron density in Supplemental Fig. S2B) and interacts simultaneously with DBD-B, DBD-C, and ssDNA, forming the keystone of a four-way interface (Fig. 1B). This four-way interface buries a total surface area of 3020 Å^2, with 860 Å^2 contributed by the linker (78% of the 10-residue linker portion becomes buried). There is also a small interface (~240 A^2) between DBD-A and the C-terminal heterotrimerization helix of DBD-C that may make a minor contribution to the stability of the quaternary structure of the 30-nt mode (Fig. 1B).

The ssDNA has 25 contiguous nucleotides that trace a U-shaped path as they traverse the DNA-binding grooves of the DBD-A, DBD-B, DBD-C, and DBD-D OB folds (Fig. 1B). DBD-A binds to the first 4 nt at the 5′ end of the ssDNA (Thy1–Thy4; top left of the "U"). DBD-B then binds to the next 5 nt (Thy5–Thy9; bottom left of the "U"), the last three of which (Thy7–Thy9) are enclosed in the four-way interface. These interact with the DBD-B DNA-binding groove, the BC linker, and a portion of DBD-C opposite from its DNA-binding groove. The ssDNA crosses over from this interface to the DBD-C DNA-binding groove over 3 nt (Thy10–Thy12). These 3 nt display poor electron density for their bases, and we presume that they are partially disordered. The DNA-binding groove of DBD-C, which is wider and longer than those of DBD-A or DBD-B, binds to the next 8 nt (Thy13–Thy20). The last 5 nt span the junction between DBD-C and DBD-D and the DNA-binding groove of DBD-D (Thy21–Thy25). This last ssDNA segment has only a subset of its base groups in well-defined electron density, consistent with the DNA affinity of DBD-D being substantially weaker than the other DBDs (Bochkareva et al. 1998; Bastin-Shanower and Brill 2001).

Table 1. *Statistics from the crystallographic analysis*

Data set	Native P2$_1$	Native C2
Resolution	35.0 Å–2.8 Å (2.9 Å–2.8 Å)	35.0 Å–3.1 Å (3.21 Å–3.1 Å)
Number of observations	89,177	88,032
Unique reflections	37,317	32,477
R_{sym}	6.8% (57.4%)	10.3% (51.2%)
$I/\sigma I$	16.1 (2.2)	11.1 (1.6)
Completeness	94.5% (97.4%)	92.3% (94.5%)
Redundancy	2.4 (2.5)	2.7 (2.7)
Refinement		
Resolution	15.0 Å–2.8 Å (2.87 Å–2.80 Å)	20.0 Å–3.1 Å (3.18 Å–3.10 Å)
Reflections ($\|F\| > 0\sigma$)	33,544	28,501
Total atoms	11,350	11,350
R factor	22.2% (31.6%)	24.4% (31.1%)
R_{free}	27.8% (38.0%)	28.6% (36.8%)
R.M.S.D.		
Bond lengths	0.008 Å	0.008 Å
Bond angles	1.331°	1.136°
B factors	2.25 Å^2	2.67 Å^2

$R_{sym} = \Sigma_h\Sigma_i |I_{h,i} - I_h|/\Sigma_h\Sigma_i I_{h,i}$ for the intensity (I) of i observations of reflection h. R factor = $\Sigma||F_{obs}| - |F_{calc}||/\Sigma|F_{obs}|$, where F_{obs} and F_{calc} are the observed and calculated structure factors, respectively. R_{free} = R factor calculated using reflection data chosen randomly (4.0% of the $P2_1$ and 5.0% of the $C2$ data) and omitted from the start of refinement. (R.M.S.D.) root mean square deviations from ideal geometry and variations in the residual B factors of bonded atoms after TLS refinement. Numbers in parentheses indicate the highest-resolution shells and their statistics.

The structures of the individual DBDs of the *U. maydis* Rpa are very similar to those of the corresponding domains in the human RPA DBD-A–DBD-B–$(dC)_8$ and DBD-C–DBD-D–RPA14 heterotrimerization core crystal structures (Bochkarev et al. 1997, 2002). They can be superimposed with root mean square deviations (R.M.S.D.s) of 0.9–1.3 Å in the positions of their Cα atoms (ranging from 105 residues for DBD-A to 163 for DBD-C). However, as discussed below, the arrangement of DBD-A relative to DBD-B differs in the 30-nt-mode structure.

DNA contacts by DBD-A–DBA-B

As in the structure of the 8-nt-mode DBD-A–DBD-B–$(dC)_8$ complex, the DBA-A and DBD-B OB folds bind to DNA using a groove made up of the β2 and β3 strands at the bottom and the L12 and L45 loops flanking the two sides, with the ends open to allow for the entry and exit of the ssDNA (Bochkarev et al. 1997; Theobald et al. 2003). Key DNA contacts are made by four aromatic or hydrophobic residues at analogous positions of the two OB folds (on β2, β3, L12, and L45) (Supplemental Fig. S3; Bochkarev et al. 1997). These residues stack with the ssDNA bases or make van der Waals contacts to base or sugar groups (Fig. 2; Supplemental Fig. S4A,B). In the 8-nt-mode structure, the DNA conformation and contacts made by the four residues are very similar across DBD-A and DBD-B (Bochkarev et al. 1997). In the 30-nt-mode structure, in contrast, the DNA conformation differs between DBD-A and DBD-B, and consequently, only a subset of the contacts made are equivalent (discussed in the legend for Supplemental Fig. S4B).

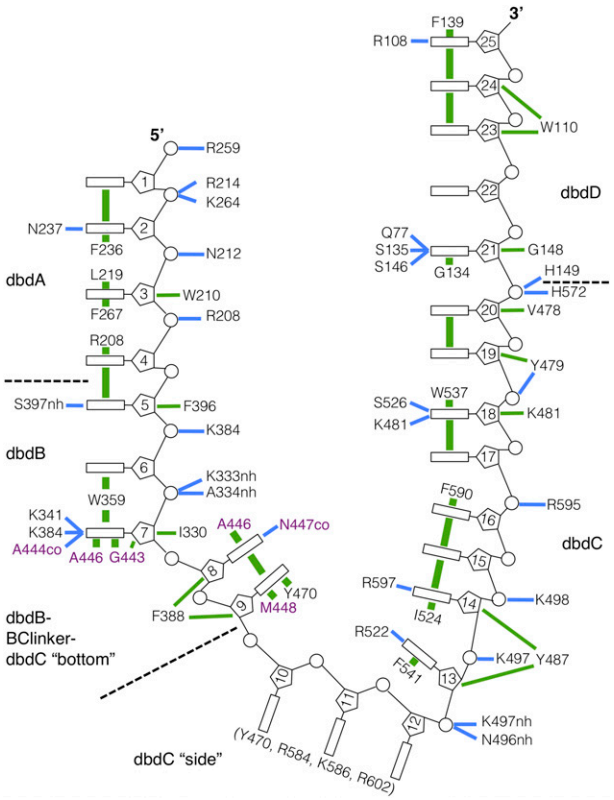

Figure 2. Schematic representation of the Rpa–ssDNA contacts. Blue lines indicate hydrogen bond and electrostatic interactions between Rpa side chains and ssDNA phosphate (circles) and bases (rectangles). Green lines indicate van der Waals contacts to base or ribose groups as well as stacking between adjacent bases (green lines connecting rectangles). The boundaries of the four DBDs are indicated by dashed lines.

BC linker conformation and DNA contacts

The nonequivalent contacts of the 30-nt mode are due at least in part to the BC linker, which, by inserting into the DNA-binding groove of DBD-B, precludes the DNA adopting the conformation observed in the 8-nt-mode structure. The linker forms two consecutive β turns (residues 443–446 and 447–450), each containing an i + 3 backbone carbonyl-amide hydrogen bond (Fig. 3A,B). The first β turn has a nearly planar shape owing to its glycine and alanine residues (Gly443–Ala444 and Gly445–Ala446), a sequence feature that is conserved in human RPA (Gly435–Val436–Gly437–Gly438) (Fig. 3A; Supplemental Fig. S3). The planar β turn inserts into the part of the DBD-B groove where a base binds in the 8-nt-mode structure (Bochkarev et al. 1997). One face of the β turn packs with the L45 residue Phe388, while the other face packs with the Thy7 base group. Almost all of the atoms of the four-residue turn make hydrogen bond or van der Waals contacts to either DNA (Thy7 and Thy8) or side chain and backbone groups inside the DNA-binding groove of DBD-B (Fig. 3A). The planar β turn essentially ejects the Thy8 nucleotide from where it would be in the 8-nt-mode structure, displacing it away from the DBD-B groove and toward DBD-C, where its base stacks with that of Thy9. The Thy8–Thy9 ribose and base groups are sandwiched between the first linker β turn and DBD-B (Phe388) at one end and DBD-C (Tyr470) at the other end (Fig. 3A,B). The second β turn of the linker anchors DBD-B onto a DBD-C surface opposite from its DNA-binding groove through van der Waals and hydrogen bond contacts to both OB folds and the edges of the Thy8–Thy9 bases that are positioned between the two DBDs (Fig. 3B). The conformational change in the BC linker and the ssDNA as well as the involvement of the DBD-C portion distal to the DNA-binding groove in the four-way junction suggest that the transition from one binding mode to the other is more complex than the simple sequential engagement of the four DBDs.

To assess the importance of the BC linker structure for the 30-nt DNA-binding mode, we mutated Gly443 and Gly445 to isoleucine. The Cα atoms of these two glycine residues make extensive intra- and intermolecular contacts in environments that do not have space for a side chain and, in the case of Gly445, adopt a backbone conformation only accessible to a glycine (Fig. 3A). The G443I/G445I double mutant binds to $(dT)_{32}$ with an ~2.5-fold weaker Kd than the corresponding wild-type protein (Supplemental Fig. S5). The decrease in the DNA affinity is comparable with the 2.6-fold to threefold reductions reported for single or double mutations in key DNA-

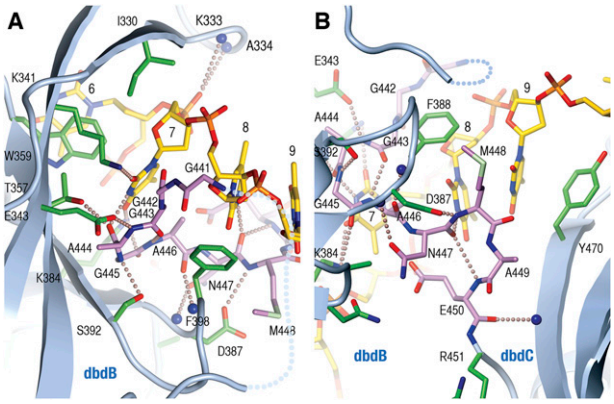

Figure 3. The BC linker adopts a two-β-turn structure stabilized by extensive hydrogen bond networks and van der Waals contacts within the linker with other DBD-B and DBD-C side chain and backbone groups as well as with DNA. (*A*) Close-up view focusing on the N-terminal β turn of the BC linker. The linker is in magenta, the DBD-B cartoon representation is in light blue, the DBD-B side chains are in green, and ssDNA is in yellow. For DBD-B, only side chains that contact the BC linker or the DNA are shown. Pink dotted lines indicate hydrogen bond and electrostatic interactions. Atoms are colored red for oxygen and dark blue for nitrogen. Small spheres indicate backbone amide nitrogen atoms involved in hydrogen bonds. View is related to that of Figure 1B by an ~90° rotation roughly about the horizontal axis. (*B*) Close-up view of the second β turn of the BC linker, colored as in *A*. View is related to that of Figure 1B by an ~180° rotation roughly about the horizontal axis, essentially looking from below the plane of that figure.

contacting residues for DBD-C (discussed in the next section) (Bastin-Shanower and Brill 2001; Cai et al. 2007).

DBD-C–DNA contacts

After the four-way interface, a 3-nt segment (Thy10–Thy11–Thy12) runs along the side of DBD-C toward its DNA-binding groove (Figs. 1B, 2). This segment is in the vicinity of several conserved basic residues, although the poor electron density of the base groups indicates that it is loosely bound. The well-ordered DNA resumes at Thy13 and extends for 8 nt across DBD-C. The ssDNA segment bound by DBD-C is nearly twice the length of that bound by DBD-A or DBD-B and traces a noncanonical DNA-binding groove that is wider in the middle and longer at the exit end compared with DBD-A/B (Fig. 4A).

The increased groove width is due to the L12 and L45 loop segments being recessed away from the center of the groove (Fig. 4A). The L12 segment also contains a 28-residue insertion that folds into a zinc-stabilized, three-β-strand structural domain (Zn domain). The Zn domain provides additional contacts to the phosphodiester backbone of the DNA (Asn496/Lys497 backbone amide and Lys497/Lys498 side chain groups) (Fig. 4B). These contacts and, in particular, the hydrogen bonds that the Asn496 and Lys497 backbone amide groups make to the phosphate group of Thy13 may facilitate the initial DBD-C–ssDNA association by stabilizing the transition from the loosely bound Thy10–Thy12 segment to the well-defined Thy13 at the groove entrance. Consistent with the Zn domain making a major contribution to DNA-binding, zinc-chelating agents dramatically reduce the affinity of DBD-C for DNA (Bochkareva et al. 2000).

The wider groove is associated with a very different DNA backbone path. Whereas in DBD-A/B, the DNA runs along the length of the groove, in DBD-C, it follows an S-shaped path, with the middle of the "S" (Thy14–Thy15–Thy16) running from the L12 side to the L45 side, nearly orthogonal to the direction of DBD-A/B-bound DNA (Fig. 4A,B). This DNA portion also has all three bases stacking consecutively, whereas, at most, two bases stack at DBD-A/B (Figs. 1C, 4B).

Even though the DNA conformation and number of bases contacted differ from those of DBD-A/B, DBD-C still uses the same set of four positions to contact the DNA as DBD-A and DBD-B. The β3 position Phe541 stacks with the Thy13 base, and the L12 position Tyr487 packs with the ribose groups of Thy13 and Thy14 (Fig. 4B). After the Thy13 base, the Thy14–Thy15–Thy16 triplet stacks with the β2 position Ile524 (Leu219 in DBD-A) at one end and the L45 position Phe590 at the other end (Phe267 in DBD-A). In contrast to these three bases in

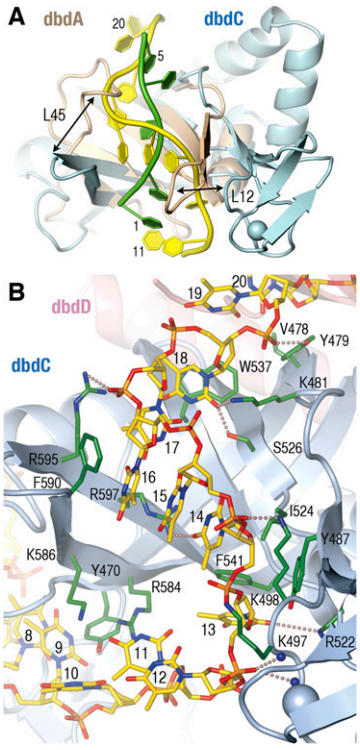

Figure 4. DBD-C has an expanded DNA-binding groove that contacts eight contiguous nucleotides. (*A*) Comparison of DNA-binding grooves and bound DNA from the DBD-A and DBD-C portions of the complex. The L12 and L45 loop segments that mark the sides of the DNA-binding grooves are indicated by arrows. The nucleotides in the two subcomplexes are numbered as in Figure 1B. (*B*) Rpa–DNA contacts at DBD-C are colored as in Figure 3A. DBD-D of Rpa32 is in pink. Only residues involved in DNA contacts are shown.

DBD-C, DBD-A has a single base (Thy3) sandwiched between these two positions. RPA mutations corresponding to F541A/F590A of *U. maydis* Rpa reduce DNA affinity by a factor of 3 (Bastin-Shanower and Brill 2001).

At the groove exit, the DNA curls along the curved surface of the OB fold, with two additional nucleotides (Thy19–Thy20) contacted by the side of DBD-C (Fig. 4A,B). The corresponding region of DBD-A is buried at the DBD-A–DBD-B interface and unavailable for DNA contacts. It is exposed in DBD-C because a different region, located ~15 Å away, packs with the next DBD-D. In this extension of the DNA-binding groove, Trp537 stacks with the Thy17–Thy18 pair, and Tyr479 stacks with the Thy19–Thy20 pair (Fig. 4B). The W537A mutation at the corresponding residue of human RPA reduces DNA affinity by a factor of 2.6 (Cai et al. 2007).

DBD-D–DNA contacts

The last 5 nt (Thy21–Thy25) extend along a relatively shallow DBD-D DNA-binding groove and, with the exception of Thy21, make only a handful of contacts to Rpa. The Thy21 base group interacts closely with a cluster of compact amino acids (Ser135, Ser146, and Gly134) in a β4–β5 region that is uninvolved in DNA binding in the other DBDs (Fig. 2; Supplemental Fig. S4C). The base of the following Thy22 points toward the solvent and is poorly ordered, while the last 3 nt are stacked with each other and pack with the β3 residue Trp110 (ribose groups of Thy23 and Thy24) at one end and the L45 residue Phe139 (base of Thy24) at the other. The paucity of the DBD-D–DNA contacts is associated with the absence of hydrophobic/aromatic residues at or near the canonical β2 and L12 positions and with an L12 loop that is too short to embrace the DNA at the groove side (Supplemental Fig. S4C).

Comparison of the 8- and 30-nt ssDNA-binding modes

The DBD-A–DBD-B–DNA structures in the 8- and 30-nt binding modes differ substantially in the relative orientation of DBD-A and DBD-B as well as in the overall DNA conformation and the protein–DNA contacts. Compared with the 8-nt-mode structure, the 30-nt mode has DBD-A and DBD-B rotated by ~30° about an axis near the interface between the two domains (Fig. 5A,B; Supplemental Fig. S6). While the DBD-A–DBD-B interface in the two complexes buries a comparable surface area (~840 and 910 $Å^2$ for the 30- and 8-nt modes, respectively), only a subset of the structural elements involved at each interface are common to both modes, and most of the interdomain side chain interactions are distinct.

The different relative arrangements of DBD-A and DBD-B are associated with distinct DNA conformations. When either the DBD-A or DBD-B domains of the two complexes are superimposed, there is essentially no spatial overlap between the backbone and base groups of the DNA bound at each domain (Fig. 5A,B). In addition, the 30-nt-mode DNA has a kinked conformation as it crosses the DBD-A–DBD-B interface (at Thy4–Thy5), while the 8-nt-mode DNA has an extended backbone conformation (Cyt4–Cyt5).

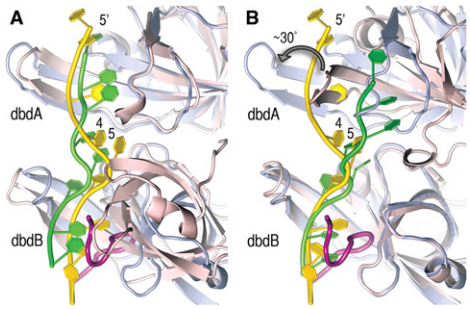

Figure 5. The relative arrangement of DBD-A and DBD-B differs in the two binding modes. (*A*) Superposition of the DBD-A–DBD-B segment of the 30-nt-mode *U. maydis* Rpa–oligo$(dT)_{32}$ complex ([blue] Rpa; [yellow] DNA) and the 8-nt-mode human DBD-A–DBD-B–oligo$(dC)_8$ complex ([pink] RPA; [green] DNA) done by aligning the DBD-A domains. Select nucleotides of the 30-nt-mode complex are labeled. The BC linker of the 30-nt-mode complex is colored magenta. The corresponding segment is absent and, presumably, disordered from the 8-nt-mode complex. (*B*) Superposition of the DBD-A–DBD-B segments of *A* done by aligning the DBD-B domains. The curved arrow indicates the 30° rotation about a point near the DBD-A–DBD-B interface that relates the two binding modes.

Some of these differences may be intrinsic to the human and *U. maydis* Rpa orthologs or may reflect the different DNA sequences in the two crystal structures. It is also possible that crystal packing may influence the relative orientation of DBD-A and DBD-B, although the four copies of the complex in our two crystal forms have the same DBD-A–DBD-B arrangement. However, at least some of the conformational change in the DNA is caused by the four-way interface because the BC linker inserts into the same region of the DBD-B DNA-binding groove that the DNA binds to in the 8-nt mode (Cyt7–Cyt8) (Fig. 5B). If the two 3′-most nucleotides of the 30-nt (Thy8–Thy9) mode adopted the conformation of the 8-nt mode (Cyt7–Cyt8), they would clash extensively with the BC linker (Fig. 5B). Conversely, it is unlikely that the 8-nt-mode nucleotides adopt the 30-nt conformation, as this would lack the stabilizing contacts provided by the BC linker and DBD-C.

Whether the different conformations in the rest of the DNA are also the result of the 8-to-30-nt-mode transition is less clear. It is conceivable, however, that the DNA conformational change at the four-way interface propagates in the 5′ direction to the DNA at DBD-B, then to the DBD-A–DBD-B interface and to DBD-A.

The DBD-A–DBD-B protein–protein interaction site

The DBD-A and DBD-B residues involved in Tag binding have been identified using chemical shift perturbation NMR methods (Jiang et al. 2006). As noted in that study, most of these residues map to a region of the 8-nt-mode DBD-A–DBD-B–$(dC)_8$ complex opposite from where the ssDNA binds to and are fully solvent-exposed. Figure 6A shows the corresponding residues of *U. maydis* Rpa mapped onto the molecular surface of the 30-nt-mode structure (the reported human RPA and corresponding *U.*

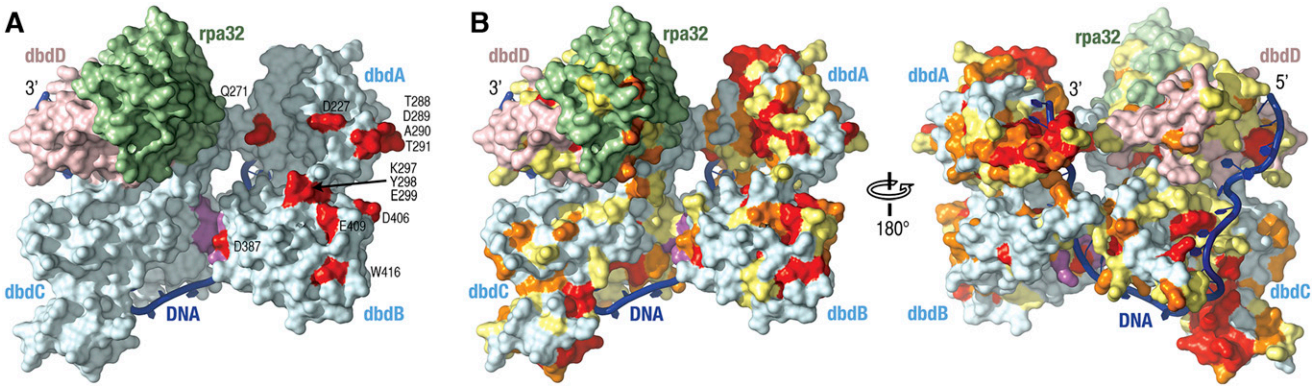

Figure 6. The residues of DBD-A and DBD-B implicated in Tag-protein interactions and the evolutionarily conserved residues that may be involved in interactions with cellular factors map to overlapping surfaces. (*A*) Molecular surface of the Rpa–oligo(dT)$_{32}$ complex in an orientation related to that of Figure 1A by an ~180° rotation about the vertical axis. The individual Rpa subunits are colored as in Figure 1B, and their domains are labeled. DNA is in blue. The *U. maydis* Rpa residues corresponding to the human RPA DBD-A–DBD-B residues implicated in SV40 Tag binding are colored in red and labeled according to the alignment in Supplemental Figure S3. (*B*) Molecular surface of the Rpa–oligo(dT)$_{32}$ complex, colored according to sequence conservation in the *U. maydis*, human, zebrafish, fly, budding yeast, and fission yeast Rpa, with red indicating identity in all orthologs. The *left* panel view is as in *A*, and the *right* panel view is as in Figure 1B.

maydis Rpa residues are marked on Supplemental Fig. S3). One of these residues, Asp387, hydrogen bonds to the BC linker and is not accessible for protein–protein interactions in the 30-nt mode (Fig. 6A; Supplemental Fig. S3). While the remaining residues are mostly solvent-exposed, several are in close proximity to DBD-C and Rpa14. The Gln271 side chain is 7 Å from the Rpa70 C-terminal helix, and Asp227 and Glu299 are within 18–20 Å of the Rpa70 C-terminal helix and the Rpa14 OB fold, respectively. This raises the possibility that the quaternary structure induced by the 8-to-30-nt transition could result in steric clashes that release the bound Tag. The Tag domain that binds to DBD-A–DBD-B is the 140-residue origin-binding structural domain (OBD), which, in principle, is large enough for such steric hindrance (Meinke et al. 2007). In addition, as Tag contacts both DBD-A and DBD-B, the relative arrangement of these two domains would be an important determinant of binding. If, as discussed earlier, the 8- and 30-nt binding modes are strictly associated with different DBD-A and DBD-B relative arrangements, then the 30-nt-mode arrangement would be incompatible with Tag contacting DBD-A and DBD-B simultaneously.

Because the DBD-A–DBD-B residues involved in binding to other factors such as Pol α–primase have not been mapped, we examined the conservation of surface residues of DBD-A and DBD-B, reasoning that those involved in functionally important interactions with endogenous proteins will show a level of conservation higher than the rest of the surface residues. The left panel of Figure 6B shows that the Rpa surface opposite from the DNA-binding grooves has clusters of conserved residues that form a nearly continuous surface extending across DBD-A and DBD-B. This surface includes residues invariant across humans, fish, flies, *U. maydis*, and budding and fission yeasts (marked in red on Fig. 6B). Overall, two-thirds of the invariant residues are on DBD-A and one-third is on DBD-B. The conservation here is comparable with that of the DNA-binding grooves on the opposite side (Fig. 6B, right panel). In contrast, the conservation is minimal on the surfaces of Rpa14 and of the portions of DBD-C and DBD-D outside their DNA-binding grooves (Fig. 6B, left panel). This indicates that the DBD-A–DBD-B surface opposite their DNA-binding grooves has an important role in RPA function, consistent with it being the binding site for cellular factors. This putative protein–protein interaction site is generally similar to the Tag-binding site, although there is only partial overlap between the conserved and Tag-interacting residues, consistent with the Tag–RPA association being species-specific (Wang et al. 2000). This suggests that the binding of other factors that interact simultaneously with both DBD-A and DBD-B may be regulated, similarly to Tag, through a combination of steric hindrance resulting from the 30-nt-mode quaternary structure and the DBD-A–DBD-B conformational change.

Discussion

Mechanism of DNA binding

The binding of RPA to ssDNA through the sequential engagement of the DBD-A through DBD-D domains has been suggested by a number of studies (de Laat et al. 1998; Iftode et al. 1999; Arunkumar et al. 2003; Wyka et al. 2003; Fanning et al. 2006). A comparative analysis of the DNA affinity of the 8-nt-mode DBD-A–DBD-B–DNA complex (~50 nM Kd) and those of the individual DBD-A (~2 μM Kd) and DBD-B (~20 μM Kd) domains concluded that the tethering effect of having the two DBDs connected by a short linker can account for most of the ~100-fold difference in DNA affinity between a single DBD and the DBD-A–DBD-B segment (Arunkumar et al. 2003). In this model, the binding to DNA of the first DBD, presumably

the higher-affinity DBD-A, increases the effective concentration of the other DBD at the DNA. It was thus concluded that the protein–protein interactions between DBD-A and DBD-B in the 8-nt-mode DNA complex do not make a substantial enough energetic contribution to result in cooperativity. This model is consistent with DBD-A and DBD-B having different relative arrangements and different interdomain interactions in the 8- and 30-nt modes and with the DBD-A and DBD-B relative orientation being determined at least in part by the conformation of the bound ssDNA.

Our structure suggests that once the 8-nt-mode complex forms, the DNA in the DBD-B DNA-binding groove would be well poised to recruit the adjacent BC linker for the formation of a three-way interface between DBD-B, DNA, and the BC linker. As the end of the BC linker that transitions into DBD-C is anchored to the DBD-B–DNA interface, the transient three-way interface will both form the composite protein–ssDNA surface for DBD-C binding and position DBD-C optimally for the final formation of the three-way DBD-B–ssDNA–BC linker–DBD-C interface (Fig. 3B). In this respect, the BC linker would have a precise structural role in the 8-to-30-nt-mode transition beyond just increasing the effective concentration of DBD-C near the DNA. That the engagement of the BC linker is an early step in the 8-to-30-nt-mode transition is supported by the affinity of intact RPA for 12-nt-long ssDNA being intermediate between the 8- and 30-nt modes (Bastin-Shanower and Brill 2001). Twelve nucleotides would be sufficient to form the four-way interface but not to reach inside the DBD-C DNA-binding groove (Fig. 1B).

The structure also reveals that part of the BC linker binds to the DNA-binding groove of DBD-B in a region occupied by ssDNA in the 8-nt-mode complex. This indicates that the 8-nt-mode ssDNA conformation in this region is not accessible to the 30-nt-mode ssDNA. If, as discussed earlier, the conformational change in the ssDNA propagates to the interface between DBD-A and DBD-B, then this could underlie the mechanism through which the 8-to-30-nt-mode transition alters the relative arrangement of the two DBDs (Fig. 5B).

Once the four-way interface anchors DBD-C, it will increase the effective concentration of the DBD-C DNA-binding groove near the 3′ end of the DNA emerging from the four-way interface. The 3 nt following the four-way interface, while poorly ordered in the crystal structure, are in close proximity to basic residues along the side of DBD-C, and this may have a role in directing the DNA toward the DBD-C groove (Figs. 2, 4B). In the absence of the four-way interface structure, the effective concentration of DBD-C near DNA would be substantially lower because of the flexibility of the BC linker. In addition, RPA orthologs have a variable number of poorly conserved residues N-terminal to the BC linker that increase the total length of the tether between DBD-B and DBD-C (Supplemental Fig. S3).

As has been suggested for the sequential binding of DBD-A and DBD-B to DNA, the stepwise transition from the 8- to the 30-nt mode would facilitate the overcoming of the ssDNA secondary structure (Fanning et al. 2006). The engagement of the BC linker would require the unfolding of only 2–4 nt, and the relatively small energetic cost of this unfolding is consistent with an ~20-fold increase in the affinity of RPA for 12-nt ssDNA compared with 8 nt (Bastin-Shanower and Brill 2001). The engagement of the DBD-C groove would require the unfolding of a substantially larger ssDNA segment, minimally spanning the 3 nt that lead to the groove and the 8 nt that interact with it. The comparatively larger energetic penalty may explain the modest 20-fold to 50-fold affinity increase attributed to the occupancy of the DBD-C DNA-binding groove (Bastin-Shanower and Brill 2001). Thus, compared with DBD-A or DBD-B, the relatively low intrinsic DNA affinity of DBD-C may be partially due to a slow on rate (k_{on}), reflecting the unfolding of ~11 nt of ssDNA secondary structure for one-step binding by the DBD-C groove.

Implications of conformational change for RPA function

The structure suggests two mechanisms for the allosteric coupling of the ssDNA-binding mode to protein–protein interactions at DBD-A–DBD-B. The flexible tethering between the DBD-A–DBD-B segment and the heterotrimerization core in the 8-nt mode gives way to a four-way interface that stabilizes a fixed quaternary structure in the 30-nt mode. This changes the accessibility of the major DBD-A–DBD-B protein–protein interaction site, especially if the binding involves a structural domain of the binding partner. The formation of the four-way interface is also coupled to a different relative arrangement of DBD-A and DBD-B compared with the 8-nt mode, altering the dispositions of the residues that make up the protein–protein interaction spanning the two domains. Taken together, these two mechanisms can help explain a number of observations relating to RPA's loading onto DNA, its displacement, and its ability to coordinate the arrival and departure of different factors during DNA processing.

The loading of RPA onto DNA has been investigated in the SV40 and papillomavirus replication model systems (Loo and Melendy 2004; Jiang et al. 2006). During the initiation of SV40 replication, the unwinding of the origin of replication is coupled to RPA loading by the Tag helicase (Jiang et al. 2006). In addition to the major DBD-A–DBD-B site, RPA has a second, weaker Tag-binding site on the WH domain of its RPA32 subunit (Arunkumar et al. 2005). This site, which is not known to be modulated by ssDNA binding, may act in concert with the DBD-A–DBD-B site to provide binding energy. After the SV40 Tag helicase recognizes the viral origin and unwinds it over ~8 nt, it recruits RPA, leading to a stable ternary complex containing Tag and RPA, presumably bound to DNA in the 8-nt mode (Jiang et al. 2006). RPA also stimulates the helicase activity of Tag and promotes more extensive origin unwinding (Fanning et al. 2006; Zou et al. 2006). It has been suggested that the emerging ssDNA would allow for the formation of the 30-nt-mode RPA complex and lead to the dissociation of the Tag–DBD-A–DBD-B

interactions (Fanning et al. 2006). Consistent with this model, the 30-nt structure shows that (1) a subset of Tag-interacting residues on DBD-A–DBD-B have reduced solvent accessibility; (2) the rest are in close proximity to portions of the heterotrimerization core, which may clash with the Tag OBD domain; and (3) the different relative orientations of DBD-A and DBD-B would change the relative positions of their Tag-interacting residues. The resulting destabilization of the Tag–DBD-A–DBD-B interface would then free Tag to bind to the DBD-A–DBD-B of a new apo-RPA molecule from solution. We presume that this is accompanied by the dissociation of Tag from the WH domain of the 30-nt-mode RPA and its association with the WH domain of apo-RPA. This process could then load successive RPA molecules on the emerging ssDNA (Fanning et al. 2006). A similar process may coordinate the formation of the prereplication complex by the papillomavirus E1 helicase as well (Loo and Melendy 2004).

The association of Tag with the RPA32 WH domain, while weaker than its association with DBD-A–DBD-B, has been shown to be important in facilitating the Tag-mediated replacement of RPA by Pol α–primase for Okazaki primer synthesis (Arunkumar et al. 2005). The WH-mediated interaction may provide an initial entry point of Tag to the 30-nt-mode RPA–DNA complex with an inaccessible DBD-A–DBD-B site. As Tag also binds to Pol α–primase (Gannon and Lane 1987), the concerted avidity of Tag and/or Pol α–primase for DBD-A–DBD-B and of Pol α–primase for DNA may shift the 30- to 8-nt-mode equilibrium toward the 8-nt mode, destabilizing bound RPA and exchanging it for Pol α–primase. The multiplicity of transient interactions between the three proteins and DNA appears to be important for the handoff process. Loss of one of at least three Pol α–primase regions that contact Tag disrupts the Tag-mediated exchange of RPA for Pol α–primase on ssDNA (Huang et al. 2010).

It has been suggested that the displacement of RPA from DNA during replication may also proceed sequentially through the dissociation of the DBD-D and DBD-C domains in the 3′-to-5′ direction (Fanning et al. 2006). Consistent with this, the DNA bound to DBD-D has minimal protein contacts and poor electron density, indicative of weak association. However, the 8 nt bound to DBD-C show continuously strong electron density and extensive protein contacts. If, as discussed in the previous section, the low intrinsic DNA affinity of DBD-C is partially due to a slow on rate, then the dissociation of DBD-C may be rate-limiting. It is thus conceivable that DBD-C displacement is facilitated by protein–protein interactions that reduce the stability of the 30-nt mode. For example, the encounter of a replicating Pol α–primase with RPA may shift the equilibrium to the 8-nt mode through direct interactions aided by their close proximity. Subsequent DNA synthesis could then more readily displace the weakly bound DBD-A–DBD-B segment from the DNA, followed by the replacement of the Pol α–primase-bound RPA by the next RPA on the template strand.

The allosteric modulation of the DBD-A–DBD-B site may also be involved in the RFC-PCNA-mediated switch from the low-fidelity Pol α to the high-fidelity Pol δ. This may come about when Pol α encounters an RPA molecule on the template strand that is associated with RFC. Several subunits of RFC bind to RPA70, and it is likely that a subset of these interactions involves DBD-A–DBD-B because Pol α–primase and RFC have been shown to compete for RPA binding (Yuzhakov et al. 1999). Not being able to interact with the DBD-A–DBD-B site and displace RPA, the stalled Pol α may dissociate, as the RPA–Pol α association has been shown to be required for Pol α to remain bound at the primed site (Yuzhakov et al. 1999). Pol α dissociation would then be followed by RFC binding to the DNA at the primer–template junction. In vitro studies have shown that RFC then loads PCNA, and Pol δ is recruited through interactions with both PCNA and RPA and, presumably, with DNA (Yuzhakov et al. 1999). Like Pol α, the elongating Pol δ may displace the 30-nt-mode RPA from the template strand by converting it to the 8-nt-mode complex. That the interaction of Pol δ with the RPA70 subunit involves DBD-A–DBD-B is suggested by the finding that Pol δ competes with RFC for RPA (Yuzhakov et al. 1999).

The structure of the 30-nt-mode RPA–ssDNA complex, in conjunction with previous studies, provides a mechanism for the stepwise formation of the high-affinity RPA–ssDNA complex. The structure also provides a framework for understanding how the allosteric coupling of RPA–ssDNA and RPA–protein interactions can facilitate the loading and displacement of RPA as well as the handoff process of RPA coordinating the assembly and disassembly of other factors.

Materials and methods

Protein expression and purification

Full-length and truncated versions of the *U. maydis* Rpa heterotrimer were produced in Hi5 insect cells by coexpressing the three subunits from two baculovirus vectors: one (pFastBac Dual) expressing glutathione-S-transferase (GST)-tagged Rpa32 and Rpa14, and the other (pFastBac1) expressing Rpa70. Cells were lysed in 50 mM Tris-HCl, 500 mM NaCl, 5 mM dithiothreitol (DTT), 1 mM phenylmethylsulfonyl fluoride (PMSF), and 1 μg/mL each leupeptin, aprotinin, and pepstatin (pH 8.0) at 4°C using a cell homogenizer (Avestin). The Rpa heterotrimer was purified by glutathione affinity chromatography followed by thrombin cleave of the GST tag overnight at 4°C and anion exchange chromatography. For crystallization, the protein was concentrated by ultrafiltration to ~10 mg/mL in 10 mM Tris-HCl, 300 mM NaCl, and 0.5% (v/v) glycerol (pH 8.0).

Crystallization and structure determination

Crystals were grown by the hanging-drop vapor diffusion method at 4°C. The Rpa–ssDNA complexes were prepared by mixing the purified protein with a threefold molar excess of ssDNA to a final concentration of ~6 mg/mL. Both crystal forms contain an Rpa heterotrimer consisting of residues 180–623 of Rpa70, residues 40–175 of Rpa32, and residues 1–114 of Rpa14. The *C2* crystal form was obtained with Rpa bound to $(dT)_{32}$ from a crystallization

buffer of 100 mM sodium acetate, 1.2 M sodium citrate, and 5 mM DTT (pH 7.0). For data collection, crystals were flash-frozen in 100 mM sodium acetate and 6 M sodium formate (pH 7.0). The $P2_1$ crystal form was obtained with Rpa bound to $(dT)_{62}$ from a crystallization buffer containing 25% (w/v) PEG 1500, 100 mM MES-imidazole-boric acid (MIB) buffer (pH 6.0), and 5 mM DTT. They were flash-frozen in crystallization buffer supplemented with 20% (v/v) ethylene glycol. Diffraction data were collected at the ID24E beamline of the Advance Photon Source and processed using the HKL2000 suite (Otwinowski et al. 2003). Both crystal forms contain two Rpa–ssDNA complexes in the asymmetric unit. Initial phases were obtained by the molecular replacement (MR) method using the structure of the human RPA heterotrimerization core (1L1O) as the search model with the program PHASER (Collaborative Computational Project, Number 4 1994). Inspection of the initial MR solution indicated shifts in the relative positions and orientations of the individual OB folds (Rpa70 DBD-A, Rpa32 DBD-D, and Rpa14 OB fold) and the C-terminal three-helix bundle (one helix from each subunit), and these shifts were consistent across the two copies of the model in the asymmetric unit. The fit of these individual domains was improved by rigid body refinement with the program PHASER and refinement with REFMAC5 (Collaborative Computational Project, Number 4 1994). Subsequently, MR was used to position the DBD-A and DBD-B domains individually using the corresponding structures from the DBD-A–DBD-B–$(dC)_8$ complex (1JMC) of human RPA as search models. Iterative cycles of model building and refinement were performed with the programs O (Jones et al. 1991) and REFMAC with TLS parameterization (Collaborative Computational Project, Number 4 1994). Refinement incorporated twofold noncrystallographic symmetry (ncs) restraints (0.05 Å R.M.S.D. in atom positions), except for a number of loops involved in crystal packing. The structure of the *C2* crystal form was determined by MR using the structure of a single copy of the Rpa heterotrimer of the $P2_1$ crystal form, in the absence of DNA, as a search model. The final refined model in the $P2_1$ crystal form contained residues 182–623 of Rpa70, 46–175 of Rpa32, and 1–112 of Rpa14. Residues 113–120 of Rpa32 and residues 86–89 of Rpa14 were disordered. For one complex in the asymmetric unit, the phosphodiester backbone of the ssDNA extended continuously from Thy1 to Thy25, with a subset of the base groups poorly ordered, as indicated in the text. For the second copy in the asymmetric unit, which overall had higher temperature factors, the ssDNA model contained Thy1 to Thy9 and Thy12 to Thy22. The portion of the DBD-D DNA-binding groove to which the last 3 nt (Thy23 to Thy25) bind in the first copy was instead involved in crystal packing in the second copy. No interpretable electron density was observed for the remainder of the nucleotides of the $(dT)_{62}$ oligonucleotide of the $P2_1$ crystal form. The *C2* crystal form contained a dimeric Rpa–ssDNA arrangement very similar to that of the $P2_1$ crystal form.

Accession numbers

Coordinates and structure factors have been deposited with the Protein Data Bank with the accession codes of 4GNX and 4GOP for the $P2_1$ and C2 crystal forms, respectively.

Acknowledgments

We thank Dr. David King of the Howard Hughes Medical Institute mass spectrometry laboratory for protein analysis, and the staff of the Advanced Photon Source NE-CAT for help with data collection. This work was supported by the Howard Hughes Medical Institute.

References

Arunkumar AI, Stauffer ME, Bochkareva E, Bochkarev A, Chazin WJ. 2003. Independent and coordinated functions of replication protein A tandem high affinity single-stranded DNA binding domains. *J Biol Chem* **278:** 41077–41082.

Arunkumar AI, Klimovich V, Jiang X, Ott RD, Mizoue L, Fanning E, Chazin WJ. 2005. Insights into hRPA32 C-terminal domain–mediated assembly of the simian virus 40 replisome. *Nat Struct Mol Biol* **12:** 332–339.

Bae SH, Bae KH, Kim JA, Seo YS. 2001. RPA governs endonuclease switching during processing of Okazaki fragments in eukaryotes. *Nature* **412:** 456–461.

Bastin-Shanower SA, Brill SJ. 2001. Functional analysis of the four DNA binding domains of replication protein A. The role of RPA2 in ssDNA binding. *J Biol Chem* **276:** 36446–36453.

Blackwell LJ, Borowiec JA. 1994. Human replication protein A binds single-stranded DNA in two distinct complexes. *Mol Cell Biol* **14:** 3993–4001.

Bochkarev A, Pfuetzner RA, Edwards AM, Frappier L. 1997. Structure of the single-stranded-DNA-binding domain of replication protein A bound to DNA. *Nature* **385:** 176–181.

Bochkareva E, Frappier L, Edwards AM, Bochkarev A. 1998. The RPA32 subunit of human replication protein A contains a single-stranded DNA-binding domain. *J Biol Chem* **273:** 3932–3936.

Bochkareva E, Korolev S, Bochkarev A. 2000. The role for zinc in replication protein A. *J Biol Chem* **275:** 27332–27338.

Bochkareva E, Belegu V, Korolev S, Bochkarev A. 2001. Structure of the major single-stranded DNA-binding domain of replication protein A suggests a dynamic mechanism for DNA binding. *EMBO J* **20:** 612–618.

Bochkareva E, Korolev S, Lees-Miller SP, Bochkarev A. 2002. Structure of the RPA trimerization core and its role in the multistep DNA-binding mechanism of RPA. *EMBO J* **21:** 1855–1863.

Braun KA, Lao Y, He Z, Ingles CJ, Wold MS. 1997. Role of protein-protein interactions in the function of replication protein A (RPA): RPA modulates the activity of DNA polymerase α by multiple mechanisms. *Biochemistry* **36:** 8443–8454.

Brill SJ, Bastin-Shanower S. 1998. Identification and characterization of the fourth single-stranded-DNA binding domain of replication protein A. *Mol Cell Biol* **18:** 7225–7234.

Cai L, Roginskaya M, Qu Y, Yang Z, Xu Y, Zou Y. 2007. Structural characterization of human RPA sequential binding to single-stranded DNA using ssDNA as a molecular ruler. *Biochemistry* **46:** 8226–8233.

Collaborative Computational Project, Number 4. 1994. The CCP4 suite: Programs for protein crystallography. *Acta Crystallogr D Biol Crystallogr* **50:** 760–763.

de Laat WL, Appeldoorn E, Sugasawa K, Weterings E, Jaspers NG, Hoeijmakers JH. 1998. DNA-binding polarity of human replication protein A positions nucleases in nucleotide excision repair. *Genes Dev* **12:** 2598–2609.

Fanning E, Klimovich V, Nager AR. 2006. A dynamic model for replication protein A (RPA) function in DNA processing pathways. *Nucleic Acids Res* **34:** 4126–4137.

Flynn RL, Zou L. 2010. Oligonucleotide/oligosaccharide-binding fold proteins: A growing family of genome guardians. *Crit Rev Biochem Mol Biol* **45:** 266–275.

Gannon JV, Lane DP. 1987. p53 and DNA polymerase α compete for binding to SV40 T antigen. *Nature* **329:** 456–458.

Gomes XV, Wold MS. 1996. Functional domains of the 70-kilodalton subunit of human replication protein A. *Biochemistry* **35:** 10558–10568.

Gomes XV, Henricksen LA, Wold MS. 1996. Proteolytic mapping of human replication protein A: Evidence for multiple structural domains and a conformational change upon interaction with single-stranded DNA. *Biochemistry* **35:** 5586–5595.

Han Y, Loo YM, Militello KT, Melendy T. 1999. Interactions of the papovavirus DNA replication initiator proteins, bovine papillomavirus type 1 E1 and simian virus 40 large T antigen, with human replication protein A. *J Virol* **73:** 4899–4907.

Huang H, Weiner BE, Zhang H, Fuller BE, Gao Y, Wile BM, Zhao K, Arnett DR, Chazin WJ, Fanning E. 2010. Structure of a DNA polymerase α–primase domain that docks on the SV40 helicase and activates the viral primosome. *J Biol Chem* **285:** 17112–17122.

Iftode C, Daniely Y, Borowiec JA. 1999. Replication protein A (RPA): The eukaryotic SSB. *Crit Rev Biochem Mol Biol* **34:** 141–180.

Jackson D, Dhar K, Wahl JK, Wold MS, Borgstahl GE. 2002. Analysis of the human replication protein A:Rad52 complex: Evidence for crosstalk between RPA32, RPA70, Rad52 and DNA. *J Mol Biol* **321:** 133–148.

Jiang X, Klimovich V, Arunkumar AI, Hysinger EB, Wang Y, Ott RD, Guler GD, Weiner B, Chazin WJ, Fanning E. 2006. Structural mechanism of RPA loading on DNA during activation of a simple pre-replication complex. *EMBO J* **25:** 5516–5526.

Jones TA, Zou JY, Cowan SW, Kjeldgaard M. 1991. Improved methods for building protein models in electron density maps and the location of errors in these models. *Acta Crystallogr A* **47:** 110–119.

Kim C, Paulus BF, Wold MS. 1994. Interactions of human replication protein A with oligonucleotides. *Biochemistry* **33:** 14197–14206.

Lao Y, Lee CG, Wold MS. 1999. Replication protein A interactions with DNA. 2. Characterization of double-stranded DNA-binding/helix-destabilization activities and the role of the zinc-finger domain in DNA interactions. *Biochemistry* **38:** 3974–3984.

Loo YM, Melendy T. 2004. Recruitment of replication protein A by the papillomavirus E1 protein and modulation by single-stranded DNA. *J Virol* **78:** 1605–1615.

Meinke G, Phelan P, Moine S, Bochkareva E, Bochkarev A, Bullock PA, Bohm A. 2007. The crystal structure of the SV40 T-antigen origin binding domain in complex with DNA. *PLoS Biol* **5:** e23. doi: 10.1371/journal.pbio.0050023.

Murzin AG. 1993. OB(oligonucleotide/oligosaccharide binding)-fold: Common structural and functional solution for non-homologous sequences. *EMBO J* **12:** 861–867.

New JH, Sugiyama T, Zaitseva E, Kowalczykowski SC. 1998. Rad52 protein stimulates DNA strand exchange by Rad51 and replication protein A. *Nature* **391:** 407–410.

Otwinowski Z, Borek D, Majewski W, Minor W. 2003. Multiparametric scaling of diffraction intensities. *Acta Crystallogr A* **59:** 228–234.

Stewart JA, Miller AS, Campbell JL, Bambara RA. 2008. Dynamic removal of replication protein A by Dna2 facilitates primer cleavage during Okazaki fragment processing in *Saccharomyces cerevisiae*. *J Biol Chem* **283:** 31356–31365.

Theobald DL, Mitton-Fry RM, Wuttke DS. 2003. Nucleic acid recognition by OB-fold proteins. *Annu Rev Biophys Biomol Struct* **32:** 115–133.

Wang M, Park JS, Ishiai M, Hurwitz J, Lee SH. 2000. Species specificity of human RPA in simian virus 40 DNA replication lies in T-antigen-dependent RNA primer synthesis. *Nucleic Acids Res* **28:** 4742–4749.

Wold MS. 1997. Replication protein A: A heterotrimeric, single-stranded DNA-binding protein required for eukaryotic DNA metabolism. *Annu Rev Biochem* **66:** 61–92.

Wyka IM, Dhar K, Binz SK, Wold MS. 2003. Replication protein A interactions with DNA: Differential binding of the core domains and analysis of the DNA interaction surface. *Biochemistry* **42:** 12909–12918.

Yang ZG, Liu Y, Mao LY, Zhang JT, Zou Y. 2002. Dimerization of human XPA and formation of XPA2–RPA protein complex. *Biochemistry* **41:** 13012–13020.

Yang H, Li Q, Fan J, Holloman WK, Pavletich NP. 2005. The BRCA2 homologue Brh2 nucleates RAD51 filament formation at a dsDNA–ssDNA junction. *Nature* **433:** 653–657.

Yuzhakov A, Kelman Z, Hurwitz J, O'Donnell M. 1999. Multiple competition reactions for RPA order the assembly of the DNA polymerase δ holoenzyme. *EMBO J* **18:** 6189–6199.

Zou Y, Liu Y, Wu X, Shell SM. 2006. Functions of human replication protein A (RPA): From DNA replication to DNA damage and stress responses. *J Cell Physiol* **208:** 267–273.